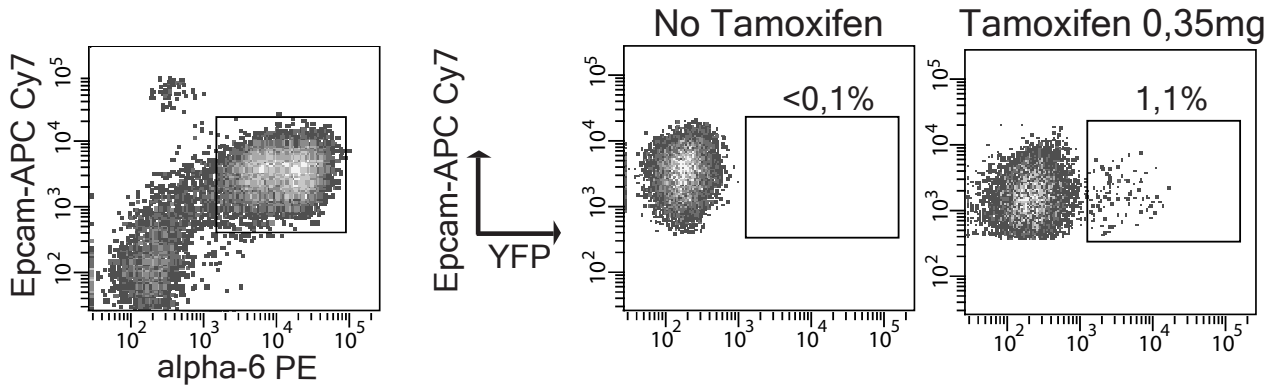


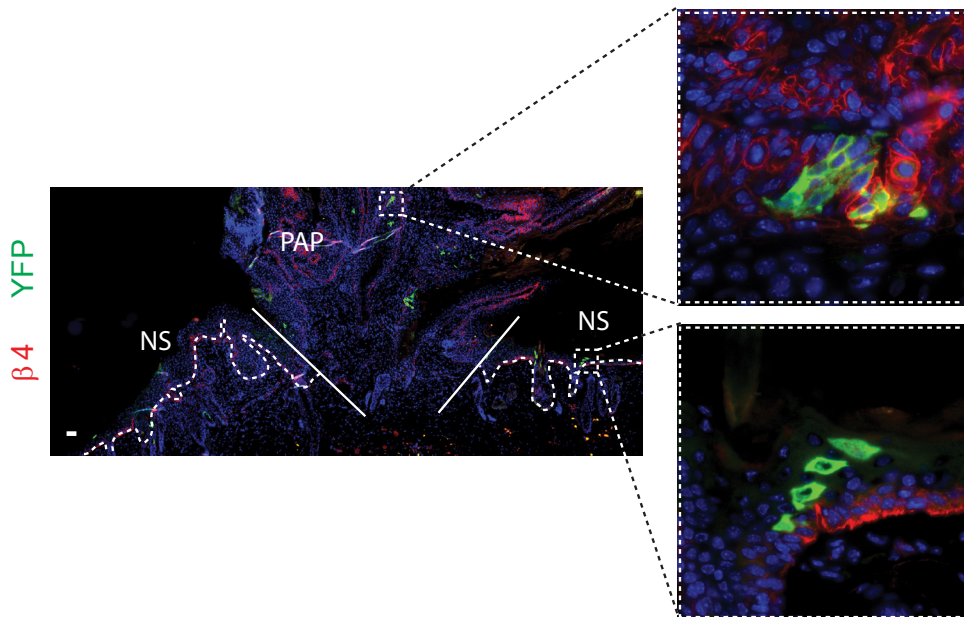
Supplementary figure 1: Papillomas are heterogeneous in size and grow mostly through basal epithelial cell expansion.

a, Co-immunostaining for $\beta 4$ integrin ($\beta 4$, red) and keratin 10 (K10, green) in a representative papilloma. Arrows point to K10+ cells from distinct suprabasal layers. b, Quantification of the average number of layers of cells expressing K10. 30 optical fields (40X) from 16 different papillomas were analyzed to quantify the number of K10+ layers. The different papillomas were pooled in 3 groups based on their surface section (<3mm² n=5 ; 3-6mm² n=5; and >6mm² n=6).c, Measure of the papilloma growth over time shows that the surface doubles in about a month (n=31 papilloma). d, Immunostaining for K10 and $\beta 4$ -integrin in representative papillomas shows that the proportion of differentiated cells does not increase with the size of papilloma; scale bars represent 500 μ m. e, Heterogeneity of size of papillomas following DMBA/TPA treatment. Scale bar represents 50 μ m, in each picture, Hoechst nuclear staining is represented in blue. “str” means “stroma”, “epi” means “epithelium” and “cor” means “stratum corneum”. Error bars denote SEM.



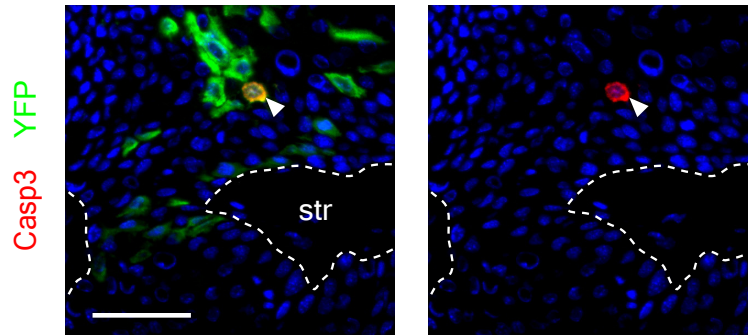
Supplementary figure 2 : A low dose of tamoxifen induces YFP expression in a low percentage of tumour epithelial cells.

FACS quantification of the percentage of YFP expressing basal tumour epithelial cells (Epcam and a6-integrin positive) before and after TAM administration. The data show that the genetic labelling system does not lead to marked cells in the absence of TAM, and that YFP expression occurs in a limited number of TECs 3,5 days after TAM administration.



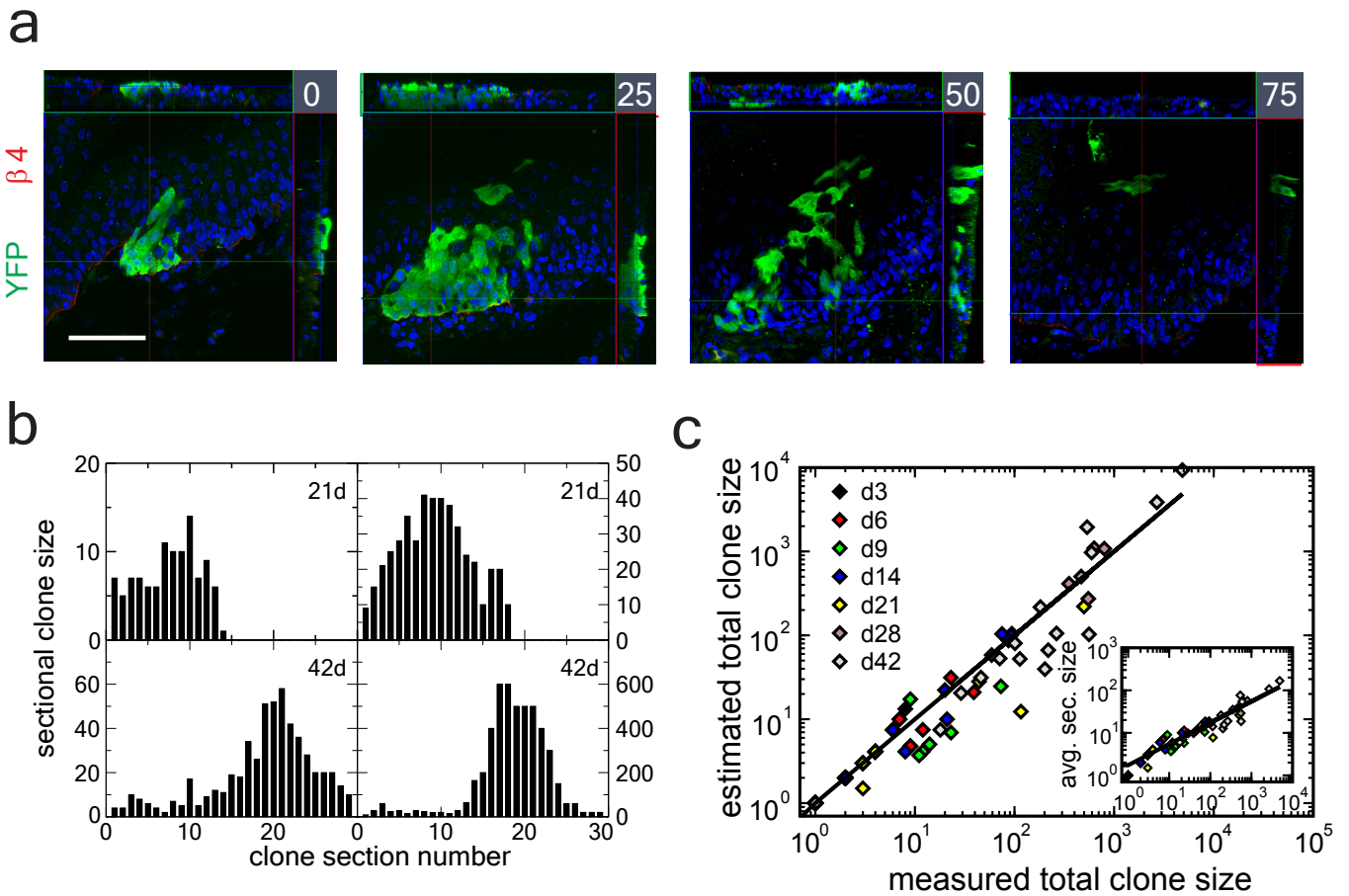
Supplementary figure 3: YFP clones induced in normal skin do not migrate and participate to tumour growth.

Immunostaining for YFP (green) and beta4-integrin (red) in a representative papilloma 9 days after induction shows that YFP clones induced in the normal skin (NS) are smaller than YFP clones within the tumour and do not migrate within the tumour. Hoechst nuclear staining is represented in blue; scale bar represents 50µm.



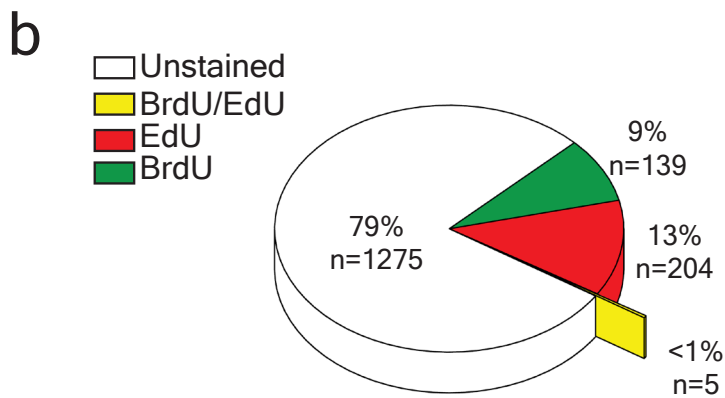
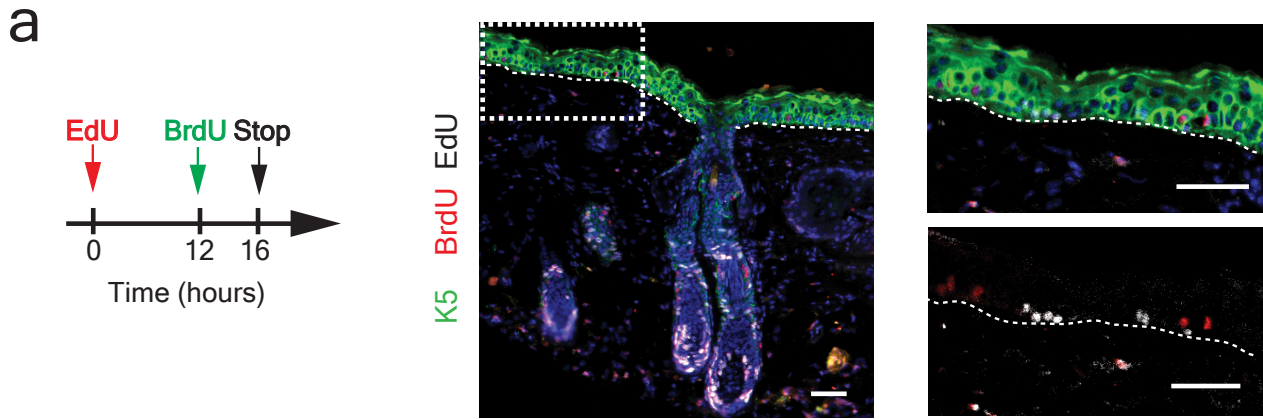
Supplementary figure 4: Apoptosis is very rare in papilloma

Immunostainings for active caspase3 (red) and YFP (green) in papilloma show an isolated apoptotic cell within a clone. Quantification of the proportion of active caspase3 positive tumour epithelial cells revealed that only 0,28% \pm 0.03% of the tumour cells are active caspase-3 positive (n=5611 cells from 3 distinct tumours). Scale bar represents 50 μ m, in each picture, Hoechst nuclear staining is represented in blue. "str" means "stroma".



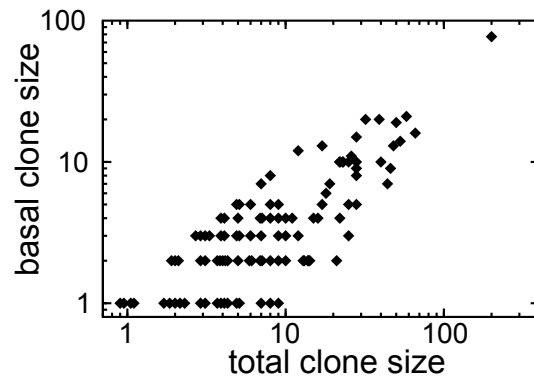
Supplementary figure 5: Estimation of the total clone size distribution in papilloma based on sectional data

a. Three-dimensional reconstruction of a YFP tumour clone analyzed by confocal microscopy on serial tumour thick sections 14 days post TAM administration allowing the quantification of the total number of YFP positive cells within a clone. b. Typical sectional clone sizes derived from a sequence of serial 25 micron sections for four clones, two at 21 days post-labelling and two at 42 days. c. Data show total clone size estimated from the average sectional cell number against the measured clone size for the clones shown in 2c (see main text and Supplementary Theory). The line $y=x$ is a guide for the eye. Inset: Data show average sectional clone size against the measured total clone size showing the predicted quadratic dependence (see supplementary theory). The line $y=(3x)^{1/2}$ is a guide for the eye. Scale bar represents $50\mu\text{m}$, in each picture, Hoechst nuclear staining is represented in blue.



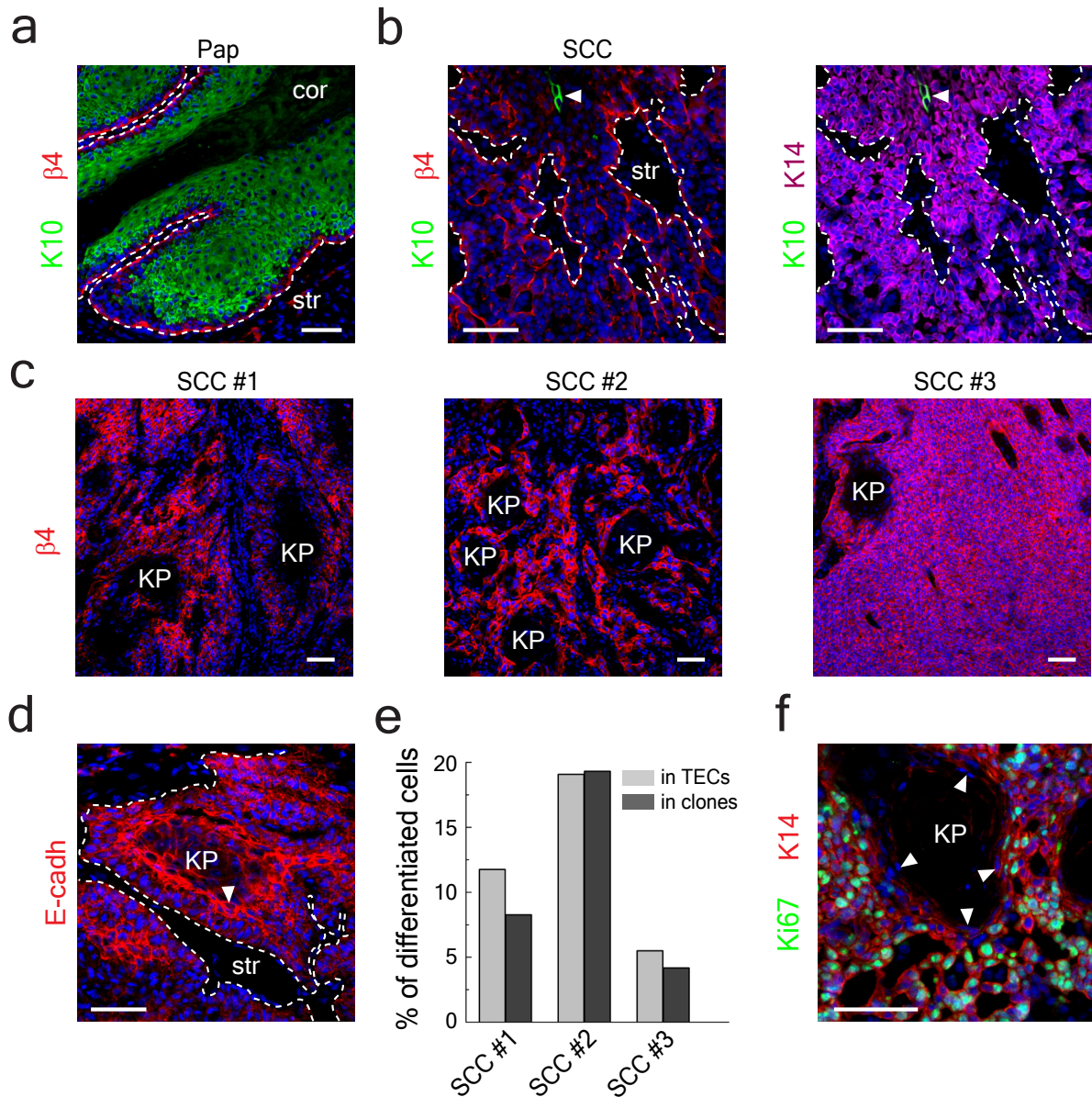
Supplementary figure 6 : Proliferation kinetic analysis in normal skin adjacent to the tumour using BrdU/EdU double labeling.

a, Immunostaining for BrdU, EdU and K5 in normal skin adjacent to papilloma from mice treated with EdU (pulse) chased for 12h, followed by a BrdU injection and another 4h chase shows extremely rare BrdU/EdU double labeled cells. Hoechst nuclear staining is represented in blue; scale bars represent 50µm. b, Quantification of the proportion of unmarked cells, BrdU, EdU and EdU/BrdU double labeled cells within the basal layer of normal skin adjacent to papillomas (n=1623 basal cells from 4 independent mice).



Supplementary figure 7 : Basal/total cell distribution in clones from papilloma after 9 days of induction.

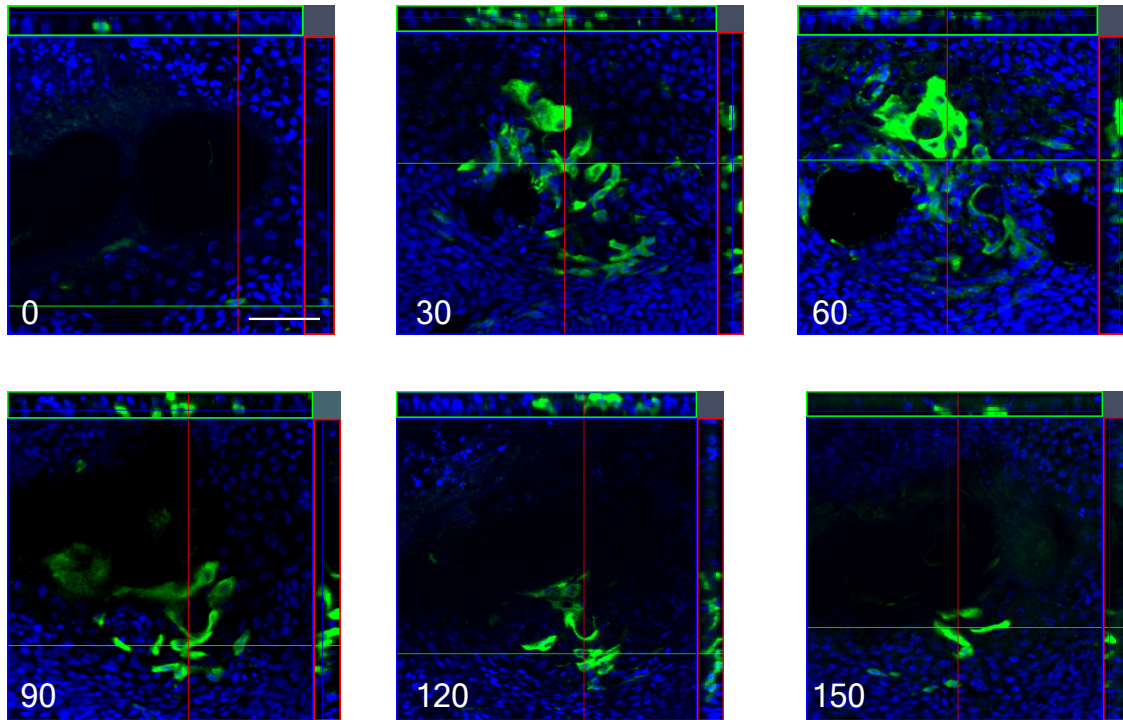
Data show basal and total sectional clone size of $n=103$ clones from 7 different papilloma at 9 days post-labelling. Note the abundance of small clones with few basal cells (derived from progenitor cells), alongside large clones with a high basal cell content (rooted in CSCs).



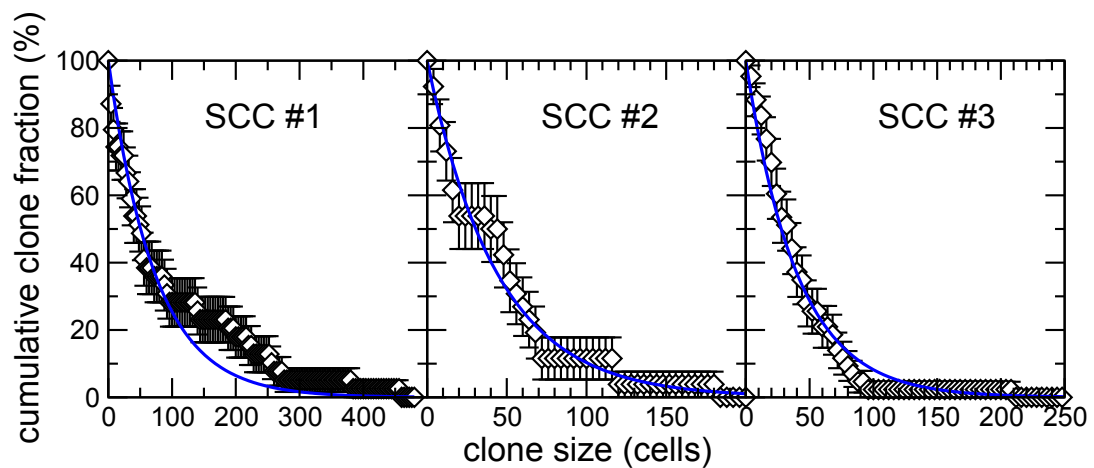
Supplementary figure 8: SCCs contain a minor fraction of differentiated cells

a, Co-immunostaining for $\beta 4$ integrin ($\beta 4$, red) and keratin 10 (K10, green) in a representative papilloma. b, Co-immunostaining for $\beta 4$ (red) and K10 (green) in a representative SCC. The arrow points to extremely rare K10+ cells. Co-immunostaining for K14 (purple) on the same slide confirms that all the cells, which are positive for $\alpha 6$ integrin but negative for K10, are tumour epithelial cells. c, Immunostaining for $\beta 4$ integrin (red) in three distinct SCCs. d, Immunostaining for E-Cadherin in a representative SCC shows cells expressing a high level of E-cadherin near a keratin pearl with a differentiated like phenotype. e, Quantification of the proportion of cells surrounding keratin pearls having a differentiated-like morphology characterized by a large size, flat shape, expressing a high level of E-cadherin, despite the absence of K10 expression within all tumour epithelial cells (light gray) or within individual YFP+ clones (dark grey). These data show that the average number of differentiated cells varies from tumour to tumour. The similar proportion of differentiated cells of the clonal analysis suggest that the targeted clones reflect the cell heterogeneity found in SCC. f, Co-immunostaining for K14 and the cell cycle marker Ki67 in a representative SCC shows the expression of Ki67 in the vast majority of tumour cells but not in the cells surrounding the keratin pearls (arrows). Scale bar represents 50 μ m, in each picture, Hoechst nuclear staining is represented in blue. “str” means “stroma”, “KP” means “keratin pearl” and “cor” means “stratum corneum”.

a



b



Supplementary figure 9 : clones of SCC TECs are spread along several serial sections after 9 days of induction

a, Immunostaining for YFP (green) performed on 6 serial sections of 30 μ m. **b**, Cumulative clone size distribution derived from the serial reconstruction of 3 distinct SCCs at 9 days post-labelling shown in Fig. 3g (data) alongside an exponential fit (blue line). For details of the fit, see Supplementary Theory. Hoechst nuclear staining is represented in blue; scale bars represent 50 μ m. Error bars denote SEM

Supplementary Methods: Theory

To address the problem of clonal evolution inside the papilloma, we have developed a biophysical modeling scheme. In the following Supplementary Methods section, we set out a more thorough discussion of the elements of this scheme, reporting only the principle conclusions in the main text. To orient our discussion, in section 1, we will begin with some preliminary remarks that follow from the analysis of the full 3d clonal reconstructions that help to constrain the modeling scheme. However, to develop a more quantitative analysis, it is necessary to increase the size of the statistical cohort of clones. To achieve this, in section 2, we will show how measurements of the sectional clone size distribution obtained from single isolated sections through the papilloma can be used to infer the corresponding statistical distribution of the total clone size, increasing the size of the statistical pool. Then, to formulate the modeling scheme, we will review briefly the known properties of keratinocytes in normal interfollicular epidermal (IFE) maintenance. This model will be used as a basis to conjecture the cellular hierarchy and fate behavior of proliferative cells inside the papilloma. In section 3, we will then describe the properties of the model and, by fitting it to the data, define the quantitative dynamics of tissue growth.

Although papilloma growth mirrors aspects of normal tissue homeostasis, the transition to squamous cell carcinoma is accompanied by further disorganization of tissue leading to invasion of the tumour mass into the dermis and the acquisition of a more three-dimensional architecture in which the stratified organization is lost. In this regime, clonal analysis reveals a qualitatively different pattern of fate behavior. In section 4, we will describe how quantitative analysis can help to resolve aspects of cell fate behavior and dynamics in this regime.

1 Clonal evolution in papilloma: basic characteristics

In homeostasis, IFE forms a stratified epithelium in which proliferating cells, confined to the basal layer, give rise to differentiating progeny which detach and rise up through the suprabasal cell layers, eventually becoming shed at the surface of the tissue. In the papilloma, this basic organization is largely recapitulated: the IFE forms a layered structure that folds in convoluted sheets (Supplementary Fig. 1). Within the mass of the papilloma, enucleated cells gradually accumulate. As in normal tissue, proliferative cells aggregate on, or near, to the basement membrane of the IFE.

Following tamoxifen administration, cells are induced throughout the epithelium. As the tissue develops and expands, some of these clones remain as single, terminally differentiated cells, while others undergo clonal expansion. To monitor the growth of these clones, we have undertaken two types of analysis. In a limited (but statistically unbiased) number of cases, we have reconstructed the entire clone from a sequence of serial $25\mu\text{m}$ sections through the tissue, allowing the total cell number inside the clones to be scored at single cell resolution. At the same time, we have accumulated a larger statistical cohort of clones from isolated $6\mu\text{m}$ sections. The 3d reconstructions provide a valuable resource from which the basic characteristics of clonal evolution can be inferred, and the larger ensemble of sectional data calibrated (see below). In particular, referring to Fig. 2c, a number of features become clear.

- First, the fraction of single cell clones remains approximately constant (at around 50%) over the first 9 days post-labelling, eventually diminishing after 14 days. This shows that the rate at which cells lose their nuclei and become undetectable is slow, on the order of once per week or less.
- Second, after just 6 days post-labelling, there are already clones with as many as 50 cells or more showing that the cell division rate of at least some of the proliferative cells is large. At the same time, large numbers of clones involve just a few cells or less suggesting that cell division can result in cell

cycle exit. This rapid expansion persists over the timecourse, with clones reaching sizes of several thousand cells after 7 weeks post-labelling.

- Finally, at 9–21 days post-labelling, the data show evidence of bimodal behavior indicative of proliferative heterogeneity. Some cells continue to give rise to colonies that have limited proliferative capacity and eventually become lost, while others progressively expand. This behavior is reinforced by the results of the sectional assay which show that the density of clones (number per unit sectional length of basal lamina) that retain a basal layer cell – referred to as “basal clones” – persist for as long as 14 days, after which there is a progressive loss (Fig. 2c).

Qualitatively, such behavior is reminiscent of the stem/progenitor cell hierarchy of normal tissue, and echos the paraclone/holoclone-type behaviour reported in culture assays. More precisely, while the epidermal progenitor cell population as a whole retains the capacity for long-term self-renewal, clones derived from individual cells are typically short-lived, giving rise to clones that stochastically expand and contract, until all of the cells have committed to terminal differentiation. By contrast, (slow-cycling) stem cells in normal tissue give rise to progenitors and tend to persist longer term.

From the 3d reconstruction, we can attempt to quantify the relative fraction of more persistent and rapidly expanding clones against the remaining fraction of smaller clones, destined to become lost. Although evidence of these two groups are manifest at just 6 days post-labelling (Fig. 2c), the separation becomes most pronounced at around 9 days where, leaving aside terminally differentiated single-cell clones, some 50% (7/14) of clones have a size of 9 cells or more, while the remaining clones have 3 cells or less. Since some of these smaller clones may have already been shed, this suggests that the majority of dividing cells labelled at induction have a progenitor-like phenotype.

Although these observations are suggestive, the data from the serial reconstruction provides only a limited resource and cannot form the basis of a reliable quantitative statistical analysis. In the following section, we will describe how sectional data can be used to acquire a definitive dataset which we will use to develop a more exacting biophysical model of the proliferative cell dynamics within the papilloma.

2 Extrapolating total clone size from sectional data

To acquire a statistical cohort of clones, we must develop and test a methodology to reconstruct total clone size from sectional data. Since each section used in the serial reconstruction has a width, $w \approx 25\mu\text{m}$, somewhat in excess of the typical cell size, we can expect the sectional count to reflect the true total cell count for clones less than some maximum size, n_{max} , i.e. for these clones, the labeled cells are typically contained within a single section. For clones of a size larger than n_{max} , we expect an ever-increasing fraction of the clone to lie outside a given section. Clearly, by knowing only the cell number within one given section, it is impossible to faithfully reconstruct the true *exact* total clone size for any individual clone. Uncertainties in any kind of extrapolation can arise both from the nature of the random intersection of the section with the clone (e.g. a section may intersect a clone at its “waist” or “extremity” leading to potentially disparate sectional cell numbers), as well as the potential irregularity in the shape of the clone. However, for the reasons outlined below, from the sectional cell number, we can make an estimate of the total cell number in the clone which, if chosen carefully, will generate the correct statistical distribution.

To understand how, let us consider the structure of large clones – clones with a size greatly in excess of n_{max} . Although the IFE is disorganized in papilloma, aspects of the normal structure persist. In particular, the tissue retains its stratified architecture with several suprabasal cell layers underpinned by a basal layer. As in normal tissue, once a clone has spanned the full suprabasal layer thickness, cells at the boundary lose their nuclei, and become undetectable. Large clones therefore tend to assume a “pancake-like” form, in which they expand (or contract) laterally along the basal layer, but are effectively confined in the transverse direction.

In section, these large clones appear as elongated structures which extend along the basal lamina (Fig. 2a). If we assume that the expansion of large clones is roughly isotropic within the basal layer, we can estimate the total number of cells in a clone and in a random thick section. For a clone of radius, R , and height, h , perpendicular to the basal layer, the total cell number is approximately given by $n_{3d} = \pi R^2 h \rho$, where ρ is the number density of cells (number per unit volume) within the papilloma. Of course this density will

vary in traversing from the basal to the suprabasal cell layers, but this variation is irrelevant if the density remains uniform along the basal layer. By contrast, the average cell number inside a section of width w is given by $n_{2d} = \frac{\pi}{4} \times 2Rh\rho$, where the numerical prefactor, $\frac{\pi}{4} = \frac{1}{2R} \int_{-R}^R dr \sqrt{1 - (r/R)^2}$, accounts for the random nature of the intersection of the section with the clone, i.e. sometimes a section may intersect the waist and others the periphery of the clone.

If we set n_{\max} as the typical number of cells inside a clone of radius w , i.e. one that would typically fall entirely within a given section, we have $n_{\max} = \pi(w/2)^2 h\rho$. Taken together, we can use these relations to develop an estimate for the total size of a clone from its sectional size,

$$n_{3d} = \begin{cases} \frac{n_{2d}^2}{n_{\max}} & n_{3d} > n_{\max} \\ n_{2d} & n_{3d} \leq n_{\max} \end{cases} . \quad (1)$$

As expected, the total size of a clone scales quadratically (i.e. with a power of two) with the sectional cell number. In practice, the discrete character of cells means that the crossover in behavior at $n_{3d} \simeq n_{\max}$ cannot be abrupt, but instead must convert gradually between the linear and quadratic dependence on n_{2d} over a range comparable to n_{\max} itself.

In making this estimate, we have assumed that clones assume a regular geometry with an intersection of the section that is oriented parallel to the symmetry axis. Of course, in reality, clones may be irregular and folded, while the section may be oblique. However, for any given clone, such effects will impact on the prefactor, $1/n_{\max}$, while the overall quadratic dependence on the sectional cell number will remain robust. More importantly, provided the fluctuations in $1/n_{\max}$ due to such irregularities are small, the distribution of total clone sizes will be largely unaffected.

To test this prediction, and obtain an estimate for n_{\max} , we can use the clone size data from the serial reconstruction described in the main text. From the sequence of serial sections that comprise a single clone, we can determine the typical number of cells within a single section by averaging the sectional count over the width of the clone (Supplementary Figure S5b). The experimental data, shown in Supplementary Figure S5c inset, for the clones recorded in Supplementary Figure S5b confirm that the measured total clone sizes n_{3d} for the serial reconstructed clones do indeed follow the predicted quadratic dependence (1) over the wide range of clones sizes (spanning three orders of magnitude), and across a wide range of timepoints. Indeed, from this data, an extrapolation of the quadratic fit (shown by the line) leads to the estimate of $n_{\max} \approx 3$.

Conversely, if we then use the sectional average clone number to infer the total clone size using Eq. (1), we can see from Supplementary Figure S5c that the estimate provides a close correspondence with the true total clone size data. Almost all departures are contained within a factor of 2. We therefore conclude that this approach provides the means to reliably relate the total clone size with that derived from random sectional data.

Finally, to correctly determine the clone size distribution, $P_{n_{2d}}$, defined as the chance of finding a clone of sectional size n_{2d} , we must take into account the statistical bias in the measurement. With a pancake geometry, the probability of finding a clone of radius R from a single random vertical section must scale with R leading to an increasing over-representation of larger clones. Since R scales in proportion to n_{2d} , we can remove this bias by rescaling the measured clone size distribution, $P_{n_{2d}}^{\text{exp}}$, by the factor n_{2d}/n_{\max} for $n_{2d} > n_{\max}$,

$$P_{n_{2d}} = P_{n_{2d}}^{\text{exp}} \times \begin{cases} \frac{n_{\max}}{n_{2d}} & n_{2d} > n_{\max} \\ 1 & n_{2d} \leq n_{\max} \end{cases} .$$

Moreover, to convert between the clone size distribution of sectional cell number, $P_{n_{2d}}$, and total cell number, $P_{n_{3d}}$, we must take into account the metric, i.e. since $P_{n_{3d}} dn_{3d} = P_{n_{2d}} dn_{2d}$, for $n_{2d} > n_{\max}$,

$$P_{n_{3d}=n_{2d}^2/n_{\max}} = \frac{dn_{2d}}{dn_{3d}} P_{n_{2d}} = \frac{n_{\max}}{2n_{2d}} P_{n_{2d}} = \frac{n_{\max}^2}{2n_{2d}^2} P_{n_{2d}}^{\text{exp}} . \quad (2)$$

Finally, since the 2d data is acquired from $6\mu\text{m}$ sections, as opposed to the $25\mu\text{m}$ sections used to generate the 3d reconstruction, we must further renormalize n_{\max} downwards. If we suppose that a $25\mu\text{m}$ section accommodates approximately 2 cells in the width, and a $6\mu\text{m}$ section just one, we must rescale n_{\max} from its measured value of 3 to around 2.

3 Quantitative analysis of the clonal fate data in papilloma

In previous studies of normal IFE, the analysis of clonal fate data was simplified considerably by constraints imposed by homeostasis. Under these conditions, the long-term clonal evolution is found to converge onto a simple scaling behavior where the chance of finding a clone larger than some multiple of the average size becomes independent of the chase period following induction^{14,15} – surviving clones grow in size, but their size distribution maintains the same shape. As well as constraining the underlying stochastic dynamics of the tissue-maintaining cell population, such scaling behavior also provides a signature of equipotency. Engrained heterogeneity in the long-term proliferative potential of the tissue-maintaining population would lead to the clonal accession of fit cells resulting in a departure from scaling (and homeostasis). In the non-homeostatic environment of the papilloma, we can no longer expect scaling behaviour to persist. We therefore have to look for less objective measures of the underlying cell dynamics.

In the following, we will use knowledge of the hierarchy and functional characteristics of proliferative cells in normal tissue to develop a simple hypothesis to address the clonal fate data. Fortunately, we will see that, despite the aberrant growth of the papilloma, crucial aspects of the normal regulatory machinery appear to stay intact allowing the clonal fate characteristics to be resolved. Later, we will comment on whether the data also admit to other possible interpretations.

3.1 Stem/progenitor cell hierarchy

On the basis of lineage tracing studies in transgenic mice, it has been conjectured that, in homeostasis, murine IFE is maintained by a basal layer of progenitor cell population following a pattern of balanced stochastic fate^{14,15}. On division, progenitors divide stochastically, giving rise to two dividing cells, two non-dividing cells, or one dividing and one non-dividing cell. To ensure homeostasis, the probability of the two symmetric fate outcomes must be perfectly balanced. Basal layer cells that have exited cell cycle then detach from the basement membrane and transfer into the suprabasal cell layers. Here we use the term “stochastic” to indicate that the fate outcome of any individual division is unpredictable, while the behaviour of the large population is defined by fixed probabilities. Formally, cell dynamics of this kind can be specified by the branching-type process,

$$P \xrightarrow{\lambda} \begin{cases} P & P & \text{Pr. } r \\ P & D & \text{Pr. } 1 - 2r \\ D & D & \text{Pr. } r \end{cases}, \quad D \xrightarrow{\Gamma} D^*, \quad D^* \xrightarrow{\sigma} \emptyset, \quad (3)$$

where λ denotes the progenitor cell (denoted P) division rate, and Γ denotes the stratification rate of the terminally differentiated basal layer cells (D). The balance between symmetric and asymmetric fate outcome is fixed by the parameter r . As cells (D^*) transfer through the suprabasal layers, they become shed at the surface at a rate σ .

With this paradigm, clonal evolution mirrors the dynamics of family surnames in a large population, with the chance expansion of some clones (families) compensated by the contraction and eventual extinction of others. In mouse tail epidermis, the progenitor cell division rate, λ , is approximately once per week, while $r \simeq 0.1$, from which it follows that some 80% of divisions result in asymmetric fate outcome¹⁴. Although evidence from *in vitro* assays suggests that the exquisite balance between proliferation and differentiation may be achieved through internal (cell-autonomous) regulation, in the two-dimensional system, long-term clonal evolution would be largely indistinguishable from a system in which balance followed from extrinsic regulation¹⁸. Finally, alongside this progenitor cell pool, evidence based on functional and marker based assays, particularly in human, suggest that IFE hosts an additional slow-cycling or quiescent stem cell pool.

On the basis of the clonal assay, we will conjecture that cells in the papilloma are also characterized by a proliferative hierarchy with a stem-like population supporting a progenitor-like pool. However, in contrast to the behaviour of normal epidermis, where stem cells appear to make little contribution to homeostatic turnover, we will suppose that, in papilloma, both populations are active. To this end, we will consider a model of tissue growth in which progenitor cells continue to follow balanced stochastic fate (3), while stem

cells adhere to a similar pattern of behaviour in which cell division can also lead to all three fate outcomes,

$$S \xrightarrow{\lambda_S} \begin{cases} S & S & \text{Pr. } r_S(1 + \delta) \\ S & P & \text{Pr. } 1 - 2r_S \\ P & P & \text{Pr. } r_S(1 - \delta) \end{cases} . \quad (4)$$

Here λ_S represents the division rate of the stem-like population (denoted as S), r_S controls the fraction of divisions that result in asymmetric fate outcome, and δ regulates the potential degree of imbalance towards proliferation.

With this paradigm, the dynamics of the stem/progenitor cell hierarchy can be cast in the form of a Master equation for $P_{n_S, n_P, n_D}(t)$, the probability that a clone contains n_S stem cells, n_P progenitor cells, and n_D terminally differentiated cells at a time t post-labelling,

$$\begin{aligned} \dot{P}_{n_S, n_P, n_D} = & \lambda_S [r_S(1 + \delta)P_{n_S-1, n_P, n_D} + r_S(1 - \delta)P_{n_S+1, n_P-2, n_D} + (1 - 2r_S)P_{n_S, n_P-1, n_D} - P_{n_S, n_P, n_D}] \\ & + \lambda(rP_{n_S, n_P-1, n_D} + rP_{n_S, n_P+1, n_D-2} + (1 - 2r)P_{n_S, n_P, n_D-1} - P_{n_S, n_P, n_D}) \\ & + \sigma(P_{n_S, n_P, n_D+1} - P_{n_S, n_P, n_D}). \end{aligned}$$

As in normal IFE, since we anticipate that the stratification is fast compared to the division rates, for simplicity we do not discriminate between differentiated cells in the basal cell layer D, and in the suprabasal cell layers D*. Moreover, the Master equation assumes that the timing between successive events (division, differentiation, loss) is statistically uncorrelated, with a mean set by the corresponding rates. Fortunately, effects due to non-Markovian features of the dynamics, such as the refractory period between consecutive cell divisions, or delays due to the transfer of cells through the suprabasal cell layers, will become erased after several rounds of cell division. Finally, although the Master equation is formally intractable analytically, as a linear ordinary differential equation, it is easily integrated numerically using the Euler method, and the results readily compared with the experimental data.

Before addressing the experimental data, let us comment on the predicted qualitative behaviour of such a cellular hierarchy. First, let us consider the ‘‘potency’’ of clones derived from the progenitor cell population. As in normal homeostasis, if proliferation and differentiation are perfectly balanced, the chance expansion of some clones will be compensated by the contraction of others leading to a neutral process in which the number of ‘‘surviving’’ clones progressively diminishes, while their size increases. Similarly, if the stem cell population is also balanced ($\delta = 0$), they will also follow a neutral drift-type process in which the stem cells, conserved in number, will become increasingly invested in a minority of surviving clones. However, since stem cells lead to the steady production of progenitor cells, these surviving clones will undergo a rapid (but not geometrical) expansion. Such dynamics mirrors the qualitative behaviour of the clonal assay – progenitors give rise to clones that persist only in the short-term while the stem-like cells give rise to expanding clones that are more likely to persist long-term. Finally, if the stem-like population is tilted towards proliferation, the stem cell-derived clones will undergo a biased drift process with the average number of stem cells rising exponentially fast with a rate set by the imbalance, $\langle n_S \rangle \sim \exp[2\delta r_S \lambda_S t]$. With this background, we now turn to consider clonal fate of cells inside the papilloma.

3.2 Fitting the model to the data

As defined above, the model involves a large number of seemingly adjustable parameters: the division rates, λ and λ_S , the shedding rate, σ , the frequency of asymmetrical cell divisions, set by r and r_S , the potential imbalance between stem cell proliferation and differentiation, δ , as well as the relative labelling efficiency. Fortunately, the transient behaviour of the progenitor cell-derived clones, and their relative abundance (see below), leads to a separability in clonal fate characteristics that can be observed in both the 3d reconstruction data, and in the sectional data. (In this context, note that the cumulative sectional clone size distribution shown in Figure 2f shows a kink at around 10 cells, the small clones being derived predominantly from progenitors and the large from stem cells). This means that, by focusing on the early time/small clone size dynamics, properties of the progenitor cell compartment (λ , r and σ) can be fixed largely independently of the properties of the stem-like compartment.

Turning to the experimental data, we could in principle use the extrapolation defined by Eq. (2) to infer the total clone size distributions from the sectional data, and use them to assess the validity of the model and

fix the parameters. Operationally, this would involve obtaining from the numerical solution of the Master equation the probabilities, $P_{n_{3d}}(t)$, describing the chance that a clone has a total of $n_{3d} = n_S + n_P + n_D$ cells after time t . However, to minimize the manipulation of the experimental data, we choose instead to use the theoretical result for $P_{n_{3d}}(t)$ to determine the probability distribution for the sectional cell count, $P_{n_{2d}}(t)$, and compare this directly with the experimental data. In doing so, by focusing on the early-time data (≤ 9 days post-labelling) and focussing on the majority of smaller clones (which are predominantly progenitor cell derived), we find a best fit if we take progenitor cells as representing some $80 \pm 4\%$ of the proliferative cells in the papilloma, a division rate λ of around once per 2 ± 0.2 days (several times faster than that reported for normal epidermis), a shedding rate σ of around once per 8 ± 1 days and $r = 0.1 \pm 0.02$, a figure reassuringly consistent with that reported for normal tissue.^{14,15}

Here, to account for the effects caused by the statistical variability in clone shape, we have implemented the following convolution to the theoretical distribution,

$$P_{n_{2d}}^{\text{conv.}}(t) = \frac{1}{N} \sum_{n'_{2d}=2}^{\infty} P_{n'_{2d}}(t) \exp\left[-\frac{1}{2v}(n_{2d} - n'_{2d})^2\right],$$

with N the normalization and variance $v = 0.2n_{2d}^2$, i.e. we take the typical variation in sectional size across the clone due to irregularity in shape to be comparable to the sectional size itself, a conclusion supported by the 3d reconstruction (Supplementary Figure S5b).

With the progenitor cell dynamics in hand, we can now turn to address the longer term (> 9 days post-labelling) and large clone size behaviour of the measured size distributions which are dominated by the minority stem cell fraction. From the early and rapid expansion of the largest clones, we can deduce a stem cell division rate that is significantly in excess of the progenitor cell division rate, λ . Intriguingly, the measured growth of the expanding clones is found to be sub-exponential, suggesting that, if there is an imbalance of stem cell fate towards proliferation, it must be small, i.e. $\delta \ll 1$. Indeed, a fit of the cellular dynamics to the experimental data over the wide timecourse up to 24 days post-labelling reveals an excellent fit for a stem cell division rate λ_s as high as 2 ± 0.3 per day, $r_s = 0.1 \pm 0.04$ (Fig. 3), i.e. as with the progenitor cell population, some 4 out of 5 divisions lead to asymmetric fate outcome, and $\delta = 0 \pm 0.03$. Such a small imbalance is consistent with the relatively slow growth rate of papilloma that results in a diameter doubling time of around a month, after which stem cells have undergone some 50 rounds of division (Supplementary Figure S1). Significantly, for these values of the division rates and fate probabilities, we find that the model provides an excellent agreement with the experimental data at 9 days post-labelling, where cells have been fractionated according to whether they are basal or suprabasal (see main text, Fig. 3d and Supplementary Fig. 7).

3.3 BrdU-EdU double-labelling assay

As well as the basal/total fractions, the model is also compatible with the results of the double BrdU/EdU incorporation assay (see main text and Fig. 3a,b). If we assume that the length of S-phase, T_S , is approximately the same for both progenitor and stem cells, the fraction of proliferative cells that take up label following a short pulse of BrdU (or EdU) is given by $n = n_P \lambda T_S + n_S \lambda_S T_S$. If we further assume that the basal layer is dominated by proliferative cells, experimental measurements of both BrdU (as well as EdU) expression lead to some 34% of positive cells (Fig. 3b). With some 80% of the proliferative cells belonging to the progenitor cell compartment, this translates to an S-phase of around $T_S \simeq 10.2$ hours. Applied to normal tissue, from the 10% of cells that are labelled following the same schedule (Supplementary Figure S6), we would deduce a cell cycle rate of approximately $10\% / (T_S \times 80\%) = 2$ per week, a figure compatible with that reported in the literature.

Applied to the papilloma, in a double-labeling experiment with a 12 hours chase period between EdU and BrdU incorporation, we would expect very few progenitors (with a cell division time of ca. 2 days) to take up label, while the majority of stem cells (with a division time of 12 hours) would. Indeed, the predicted fraction of double positive cells, $n_S \lambda_S T_S = 17\%$ compares favorably to the 16% of cells measured in experiment (Fig. 3b).

3.4 Discussion

In developing a modeling scheme to describe papilloma growth, we have assumed that both the progenitor and stem-like cell population conform to a cell-autonomous pattern of regulation in which fate outcome following division is seemingly uncorrelated with that of neighbouring cells. However, as mentioned above, it is important to recognize that, in the two-dimensional geometry of epidermis, the long-term clonal evolution of such a neutral process is largely insensitive to the pattern of regulation – intrinsic vs. extrinsic (cf. Ref. [19]). Neither the model, nor the data, can therefore offer useful insight on the underlying mechanism of regulation that leads to the fate behaviour of either cell population.

In summary, we have argued that the data provide evidence for proliferative heterogeneity involving a cellular hierarchy with just two compartments – a remnant of the stem/progenitor hierarchy thought to characterize normal tissue. In this paradigm, the proliferative cells within each of these two compartments function as an equipotent pool with properties that are seemingly unchanging over time. All stem-like cells have equal “fitness”, and the question of their long-term survival is simply a matter of chance. A similar remark applies to the progenitor cell pool.

In principle, heterogeneity of clonal evolution could also develop through a continuum of proliferative potential leading to the succession of “dominant” clones in a non-neutral manner. Clearly, while one allows for an unlimited degree of complexity, it is impossible to argue that the clonal fate data categorically rule out such a scenario. Indeed, each clone could be derived from individual cells following a unique programmed pattern of lineage specification leading to clones of defined size and cellular composition. However, for any model to be viable, it has to explain the fact that the clonal induction of cells in different papilloma, at different stages of development, give quantitatively similar clone size distributions over time. Equally, it has to explain the capacity of progenitors to give rise to terminally differentiated cells, and for clones to be become extinct over time. And it has to explain the apparent sub-exponential growth of more persistent clones. It is remarkable and significant that the current model involving only the smallest revision of the known behaviour of normal tissue – the activation of slow-cycling stem cells – is capable of describing the entire range of clonal fate data (basal and total size, survival probability, proliferation rates, etc.), spanning as many as fifty rounds of cell division.

4 Clonal evolution in invasive carcinoma

Finally, we turn now to consider the clonal evolution of cells within an invasive carcinoma. Referring to the main text, we have seen that the transition from papilloma to carcinoma is accompanied by a change in the morphology of the tumour. Instead of the stratified architecture, which leaves progenitor cells confined to the basal layer, the carcinoma has a more three-dimensional appearance in which the vast majority of cells remain proliferative (see main text and Figs. 4i-k). Although there is some tumour-to-tumour variability, we estimate that around $10 \pm 10\%$ of cells are terminally differentiated, and typically clustered in keratin pearls (Fig. 4 and Supplementary Figure S8).

Following induction, we traced clonal evolution of cells over a 9 day timecourse in three invasive carcinomas using K5 and K14 promoters. At this relatively early timepoint, it was possible to score the total number of cells per clone for each of these three tumours, despite their potential for fragmentation (see main text). In all cases, the clones continued to show heterogeneity in size with clones as small as 2-4 cells coexisting with clones of 400 cells or more (Fig. 4g). However, in stark contrast to the papilloma, we found just one single cell clone, consistent with the dearth of terminally differentiated cells in the tumours. Moreover, in contrast to the papilloma, the carcinoma do not show evidence for two discrete progenitor cell populations, i.e. the characteristic bimodality of the clone size distribution seen in papilloma is not recapitulated in carcinoma. Instead, there is a broad continuum of clone sizes, which translate to an exponential-like cumulative total size distribution (Supplementary Figure S9b). However, despite this exponential character, the proliferation rates appear variable, with one clone expanding by a factor of two in average more than the two others.

Although variability in clone sizes would accommodate a number of possible interpretations, including engrained proliferative heterogeneity in the tumour-maintaining population, such behavior can also be explained by the geometric expansion of a single progenitor cell population with a broad (Poisson) distribution

of cell cycle times defined by the process,

$$C \xrightarrow{\lambda_C} \begin{cases} C & C & \text{Pr. } R(1 + \Delta) \\ C & D & \text{Pr. } 1 - 2R \\ D & D & \text{Pr. } R(1 - \Delta) \end{cases}, \quad D \xrightarrow{\gamma} \emptyset, \quad (5)$$

where λ_C denotes the division rate of the tumour cells (denoted by C), R controls the fraction of divisions that result in asymmetric cell fate, Δ the imbalance towards differentiation, and γ the rate at which terminally differentiated cells enucleate. Here we have assumed that apoptosis makes a minimal contribution to tumour growth, consistent with measurements of caspase3 expression (Supplementary Figure 4).

If we restrict attention to the progenitor cell fraction, which dominates the total clone size, we can consider the simplified process of symmetric self-renewal and loss,

$$C \xrightarrow{2R\lambda_C} \begin{cases} C & C & \text{Pr. } (1 + \Delta)/2 \\ \emptyset & & \text{Pr. } (1 - \Delta)/2 \end{cases}. \quad (6)$$

In this case, the clone survival probability is given by

$$P_{\text{surv.}}(t) \equiv 1 - P_0(t) = \frac{1 - (1 - \Delta)/(1 + \Delta)}{1 - (1 - \Delta)/(1 + \Delta)e^{-2R\Delta\lambda_C t}} = 1 - \left(\frac{1 - \Delta}{1 + \Delta}\right) (1 + e^{-2R\Delta\lambda_C t}) + O(e^{-4R\Delta\lambda_C t}),$$

while the corresponding clone size distribution is given by $P_n^{\text{surv.}}(t) = (1 - \eta(t))\eta^{n-1}(t)$, where $\eta(t) = \left(\frac{1+\Delta}{1-\Delta}\right) P_0(t)$. From this result, we can deduce that the cumulative size distribution takes the form of an exponential,

$$C_n(t) = 1 - \sum_{m=1}^n P_m^{\text{surv.}}(t) = \eta^n(t) = e^{-n/\ln(1/\eta(t))}.$$

In particular, at long times, $2R\Delta\lambda_C t \gg 1$, $\eta(t) \simeq 1 + e^{-2R\Delta\lambda_C t}$ and the distribution takes the simple exponential form,

$$C_n(t) \simeq e^{-n/\langle n_C(t) \rangle},$$

where $\langle n_C(t) \rangle = e^{2R\Delta\lambda_C t}$ denotes the average size of surviving clones.

With so few terminally differentiated cells, and no terminally differentiated clones, we are led to conclude that few, if any, cell divisions result in terminal divisions (i.e. $\Delta \simeq 1$). Moreover, if we assume that the rate of loss, γ , remains low, the frequency of asymmetrical cell divisions must also be small, $R \simeq 1/2$. In this limit, we can use the fit of the model to the data to estimate the approximate rate of cell division. With $\langle n_C \rangle \simeq 73 \pm 10$ for one tumour, and $\langle n_C \rangle \simeq 42 \pm 5$, we estimate cell division rates, λ_C , of around once per two days. This figure is consistent with the results of the EdU/BrdU assay which shows that, 12 hour after a short EdU pulse, a BrdU pulse labels less than 2% of EdU+ cells (Fig. 4n).